SYNTHESIS OF Mn_3O_4 NANOPARTICLES AND THEIR APPLICATION TO CANCER CELLS

Marijan GOTIĆ[1,*], Siniša IVANKOVIĆ[2], Svetozar MUSIĆ[3] and Tatjana PREBEG[4]

Ruđer Bošković Institute, Bijenička c. 54, HR-10002 Zagreb, Croatia;
e-mail: [1] gotic@irb.hr, [2] sivankov@irb.hr, [3] music@irb.hr, [4] prebeg@irb.hr

Received April 2, 2009
Accepted July 26, 2009
Published online September 11, 2009

The Mn_3O_4 nanoparticles were synthesized by optimizing the precipitation system $MnCl_2/H_2O_2/NH_4OH$. The material thus obtained was microstructurally characterized using X-ray diffraction (XRD), Fourier transform infrared (FT-IR) spectroscopy and scanning electron microscopy (SEM). The Mn_3O_4 nanoparticles were applied to fibroblast and cancer cells. In the concentration range 25–100 μg/ml the particles showed low cytotoxic effects on L929 fibroblast cells, medium cytotoxic effects on FsaR fibrosarcoma cells and high cytotoxic effects on SCCVII carcinoma cells. *N*-Acetyl-L-cysteine (NAC) increased cytotoxicity of Mn_3O_4 nanoparticles, which suggested that reactive oxygen species (ROS) were not responsible for their selective cytotoxic effect. It was shown that the Mn_3O_4 nanoparticles entered the cancer cells and aggregated inside the membrane-bound spaces that were recognized as destroyed mitochondria.

Keywords: Mn_3O_4; Hausmannite; Cytotoxicity; Cancer cells; Nanomaterials; Electron microscopy.

Metal oxide powders can be synthesized using various wet chemistry routes such as precipitation and hydrolysis in alkaline medium[1,2], hydrolysis in acid medium[3,4], hydro- or solvothermal synthesis[5], sol-gel route[6,7], microemulsion technique[8], using esterification[7,9–11], non-aqueous route[12] and γ-irradiation assisted synthesis[8,13]. Manganese occurs in a variety of oxidation states and chemical and structural forms. Due to a variety of oxidation states as well as the facile phase transformations of MnO_x during preparation, only a mixture of various manganese oxides (MnO_2, Mn_2O_3 and Mn_3O_4) is usually obtained. In addition, manganese oxyhydroxides (MnOOH) are often associated phases in wet synthesis. Mn_3O_4 nanoparticles have found use as catalysts and electrode material. Likewise, Mn_3O_4 is a weak ferromagnetic material.

Collect. Czech. Chem. Commun. 2009, Vol. 74, No. 9, pp. 1351–1360

doi:10.1135/cccc2009047

Yang et al.[14] synthesized Mn_3O_4 polyhedral nanocrystals by a microwave-assisted technique using an aqueous solution containing $Mn(OCOCH_3)_2$ and hexamethylenetetramine. Chen et al.[15] synthesized crystalline Mn_3O_4 nanoparticles of different morphologies using liquid homogeneous precipitation with $MnCl_2$, H_2O_2, NaOH and sodium dodecylbenzene sulfonate surfactant as reactants. Zhang et al.[16] prepared crystalline Mn_3O_4 nanopowders by solvothermal treatment of γ-MnOOH nanowires in ethylenediamine and ethylene glycol. Gibot et al.[17] prepared Mn_3O_4 nanoparticles in aqueous solution using $KMnO_4$ and hydrazine as a reducing agent. Hydrophilic and hydrophobic Mn_3O_4 particles were prepared. Wang et al.[18] synthesized single-crystal Mn_3O_4 nanorods by a method starting from $MnCl_2$ and NaOH as a precipitating agent. Vázquez-Olmos et al.[19] reported one-step synthesis of Mn_3O_4 nanoparticles starting from manganese(II) acetate in aqueous dimethylformamide. Ozkaya et al.[20] synthesized Mn_3O_4 nanoparticles by a precipitation method based on the oxidation of manganese sulfate and hydrolysis with NaOH and concentrated NH_3 solution. Hu et al.[13] synthesized monodisperse Mn_3O_4 particles by γ-irradiation of manganese sulfate in the presence of a cationic surfactant.

Manganese (Mn) and Mn-derived nanoparticles, such as $MnFe_2O_4$, are among the best contrast agents for magnetic resonance imaging (MRI). However, the manganese toxicity restricted its bioimaging applications. On the other hand, due to its toxicity manganese could be regarded as antitumour agent. In this work, we report new results regarding the synthesis of Mn_3O_4 nanoparticles and their application to tumour cells. Precursor manganese(II) chloride was oxidized with H_2O_2 and then precipitated with NH_4OH. In a series of experiments (trial-and-error approach), we optimized the $MnCl_2/H_2O_2/NH_4OH$ system to obtain Mn_3O_4 nanoparticles not contamined with other manganese phases. These Mn_3O_4 nanoparticles were applied to tumour cells. It was shown that the Mn_3O_4 nanoparticles aggregated in cells inside the membrane-bound spaces that were recognized as destroyed mitochondria. With the destroyed mitochondria, the cells remained without energy, which, as a consequence, leads to the cell death.

EXPERIMENTAL

The chemicals $MnCl_2 \cdot 4H_2O$, concentrated H_2O_2 and concentrated NH_4OH solution of analytical-grade purity were supplied by Kemika, Zagreb. Double-distilled water was also used. The following procedure was employed to prepare the Mn_3O_4 nanoparticles. Into 0.2 M $MnCl_2$ (250 ml), concentrated H_2O_2 (5 ml) was slowly added dropwise under vigorous stirring at room temperature, followed by addition of concentrated NH_4OH (5 ml). The precipitation mixture was held in a closed flask in a laboratory oven at 90 °C for 24 h. The pre-

cipitate was then washed with double-distilled water and dried at 60 °C. This precipitation mixture is sensitive to the order of addition of the precipitating agents. For example, under the same conditions, if the order of addition of H_2O_2 and NH_4OH is reversed, the formation of γ-MnOOH prevails.

IR spectra were recorded at 20 °C using a Perkin–Elmer 2000 spectrometer. A sample was pressed into a small KBr disc. The XRD patterns were recorded at 20 °C using an APD 2000 (Ital Structures, Italy) X-ray powder diffractometer (CuKα radiation, graphite monochromator, NaI-Tl detector). A thermal-field-emission scanning electron microscope (FE SEM; Jeol JSM-7000F) was connected to an EDS/INCA 350 energy dispersive X-ray analyzer (Oxford Instruments).

Cells (L929, FsaR and SCCVII lines) were cultured and incubated (24 h) in the presence of Mn_3O_4 nanoparticles using standard laboratory procedures. Control cells were incubated (24 h) in a Mn_3O_4-free medium. Cells were visualized using an inverted inverse microscope (Zeiss). In order to determine the production of reactive oxygen species (ROS) in Mn_3O_4 induced cell death, L929, FsaR and SCCVII cells were pre-treated for 1 h with *N*-acetyl-L-cysteine (NAC; Sigma, Batch# 038KO7111) at final concentrations of 1, 5 and 10 mmol/l. The determination of the cell survival fraction was carried out with a UV-Vis spectrophotometer (Crystal Violet bioassay). More detailed experimental procedures can be found in the literature[21,22].

For cell substructure studies, freshly collected cells were fixed in 2% glutaraldehyde in cacodylate buffer (pH 7.2), post-fixed in 1% OsO_4 in the same buffer and, after dehydration, embedded in the Spurr resin. Ultrathin sections of the materials were stained with uranyl acetate and lead citrate and examined using transmission electron microscopy (TEM).

RESULTS AND DISCUSSION

Figure 1a shows a characteristic part of the XRD patterns of a synthesized sample. This sample is assigned in accordance with the ICDD PDF card No. 24-0374 (Mn_3O_4, hausmannite). The *hkl* indices of hausmannite (tetragonal symmetry, space group $I4_1/amd$) are given. The relative intensities as well as peak positions of the XRD patterns match perfectly with that of pure Mn_3O_4 (hausmannite). The average crystallite size of synthesized Mn_3O_4 was 20 nm, as estimated using the Scherrer equation. Figure 1b shows IR spectrum of the synthesized sample with four absorption bands at 637, 597, 532 and 416 cm^{-1}. The bands at 637, 532 and 416 cm^{-1} are in accordance with the lattice vibrations predicted for synthetic Mn_3O_4 (refs[23,24]). The band at 637 cm^{-1} is due to a ν(MnO) mode at tetrahedral sites, while the band at 532 cm^{-1} corresponds to a δ(MnO) vibration in an octahedral environment. The band at 416 cm^{-1} is due to a ν(MnO) vibration at octahedral sites. The wavenumber of ν(MnO) at tetrahedral sites of 637 cm^{-1} rather than ca. 610 cm^{-1} indicates the substoichiometric nature of the synthesized Mn_3O_4 nanoparticles. It is well known that hausmannite prepared at low temperatures contains a certain oxygen excess, expressed as

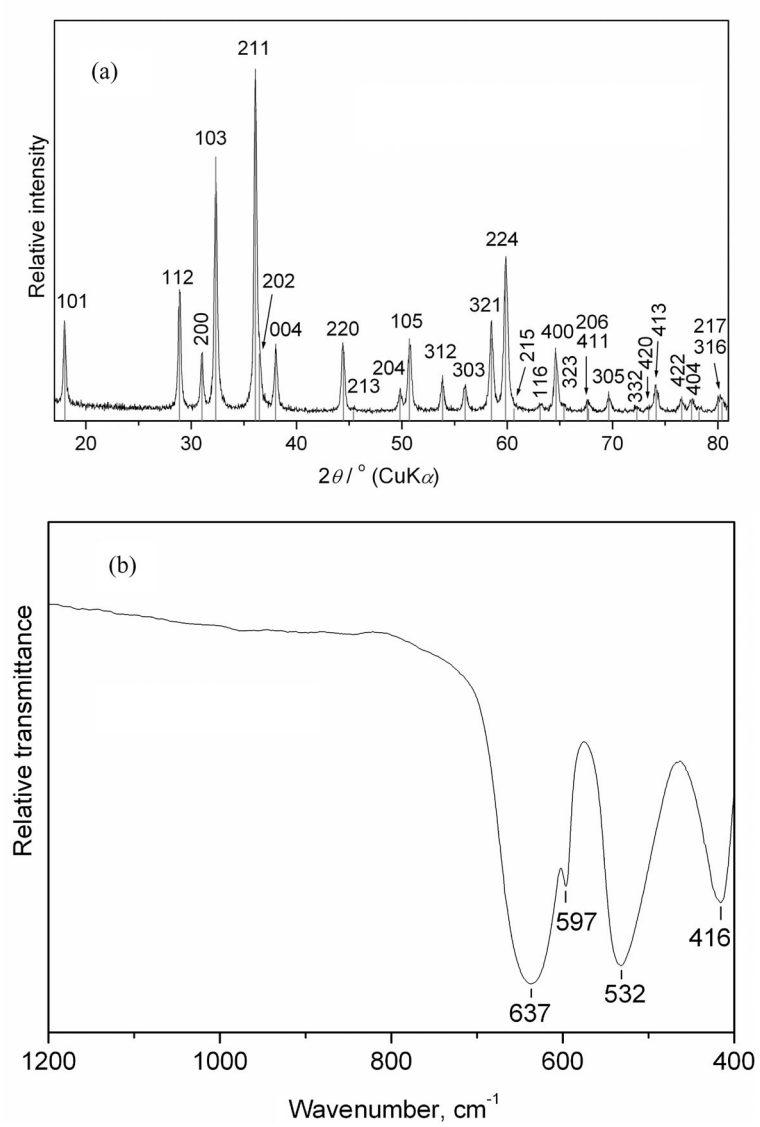

FIG. 1

XRD patterns of the synthesized 20-nm Mn_3O_4 nanoparticles (a) and the corresponding IR spectrum (b)

$Mn_3O_{4+0.5x}$, where $0 < x < 1$ ($x = 0$ for Mn_3O_4, $x = 1$ for Mn_2O_3)[25]. In this substoichiometric hausmannite, some of the tetrahedral Mn^{2+} ions are oxidized to Mn^{3+}, which causes the ν(MnO) band attributed to the tetrahedral sites at ca. 610 cm^{-1} to shift towards a larger wavenumber by up to 30 cm^{-1}. This is also in accordance with the fact that the dimensions of the nanoparticles are always more or less associated with their substoichiometric nature. The very narrow band at 597 cm^{-1} can be assigned to the lattice Mn–O vibration of manganite (γ-MnOOH). The appearance of this band in the IR spectrum and not in the XRD patterns is in accordance with much higher sensitivity of FT-IR spectroscopy to the presence of γ-oxyhydroxide polymorphs. Furthermore, this advantage is even greater in the nanosized systems, as the XRD lines broaden, while the lattice Mn–O vibration feature of γ-oxyhydroxide polymorphs remains sharp. For example, lepidocrocite, γ-FeOOH, also shows a very strong lattice Fe–O vibration at 1022 cm^{-1}, being detectable in a mixture of iron oxides by IR spectroscopy in very small amounts[26]. In the present case, γ-MnOOH was probably present in traces not detectable by XRD.

Figure 2 shows an FE SEM image of synthesized Mn_3O_4 nanoparticles. The discrete ca. 20-nm pseudospherical particles are clearly visible. There are no wire-like particles, confirming that γ-MnOOH was present only in traces.

Drying the "wet" Mn_3O_4 precipitate may cause surface precipitation of γ-MnOOH. This can also happen in the contact of Mn_3O_4 with humid air. The γ-MnOOH formation mechanism includes surface oxidation of Mn^{2+}

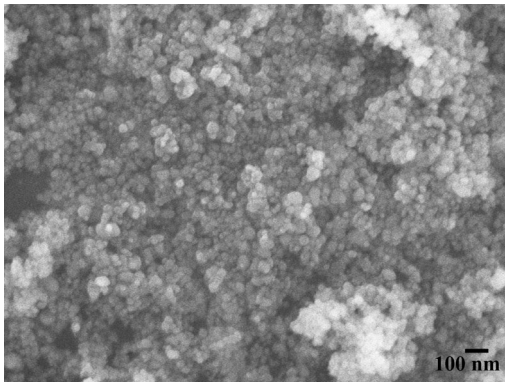

FIG. 2
FE SEM image of the Mn_3O_4 nanoparticles. The discrete ca. 20-nm pseudospherical particles are clearly visible

to Mn^{3+} ions on Mn_3O_4 particles, yielding $-Mn^{III}=O$ groups, that undergo hydroxylation with adsorbed H_2O molecules. The resulting $-Mn^{III}(OH)_2$ groups can be considered as precursors of γ-MnOOH (probably in the form of thin films), which may explain why free γ-MnOOH wires were not visible in the FE SEM image (Fig. 2).

The application of nanoparticles in biomedicine is an emerging field[27,28]. The cytotoxicity of nanosized Fe-TiO_2 (ref.[21]) and V_2O_5 (ref.[22]) nanoparticles to cancer cells was investigated previously. It was shown that V_2O_5 nanoparticles are highly cytotoxic to cancer cells *per se*, whereas Fe-TiO_2 nanoparticles had to be sensitized with UV light to be able to kill cancer cells. In this work, the synthesized Mn_3O_4 nanoparticles were applied to selected fibroblast and cancer cells. Figure 3 shows quantitative estimation of the cytotoxic effect of Mn_3O_4 nanoparticles applied to L929 fibroblast cells, FsaR fibrosarcoma cells and SCCVII carcinoma cells. The Mn_3O_4 nanoparticles showed a low cytotoxic effects on L929 fibroblast cells, medium cytotoxic effects on FsaR fibrosarcoma cells and high cytotoxic effects on SCCVII carcinoma cells. This preferential cytotoxic effect of Mn_3O_4 nanoparticles on cancer cells versus fibroblast cells is in accordance with the preferential killing of cancer and human T cells using ZnO nanoparticles obtained by Hanley et al.[29]. In order to determine the production of ROS in Mn_3O_4 induced cell death, L929, FsaR and SCCVII cells were pre-treated with NAC. Instead of the expected quenching of the ROS and increased viability of cells, NAC increased cytotoxicity of the Mn_3O_4 nanoparticles (results not shown). Thus, NAC did not confirm the production of ROS, which suggests that ROS were not responsible for the selective cytotoxic effect of the Mn_3O_4 nanoparticles. Further investigation is needed to explain the selective cytotoxic effects of the Mn_3O_4 nanoparticles. Also, NAC enhanced the Mn_3O_4 cytotoxicity and a detail mechanistic study should be undertaken to explain this absolutely unexpected reverse effect.

Figure 4 illustrates the cytotoxic effect and sub-cellular accumulation of Mn_3O_4 nanoparticles in cancer cells (SCCVII line). Figure 4a shows a microphotograph of a control cancer cell culture that contains a number of cells with well-defined morphologies characteristic of the cell culture. Figure 4b shows the effect of addition of Mn_3O_4 nanoparticles on the cancer cell culture. The concentration of Mn_3O_4 nanoparticles was 100 μg/ml (~440 μmol/l). The Mn_3O_4 nanoparticles at this concentration reduced significantly the number of cancer cells and altered their morphologies. Figure 4c shows a TEM micrograph of control cancer cells. The subcellular structure of one viable SCCVII cell is visible. Figure 4d shows a TEM micro-

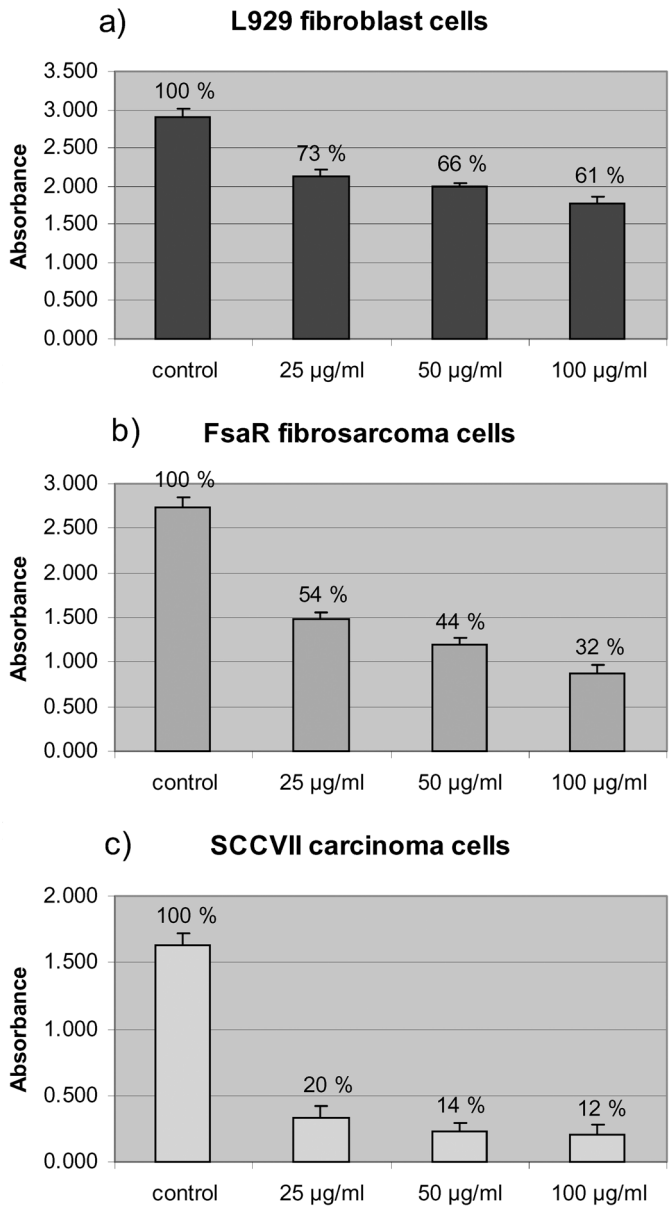

FIG. 3

Cell viability (in %) of L929 fibroblasts cells, FsaR fibrosarcoma cells and SCCVII carcinoma cells in dependence on the Mn_3O_4 nanoparticle concentration. The absorbance is proportional to the cell viability. The viability of control cells (without addition of Mn_3O_4 nanoparticles) is regarded as 100%

graph of Mn_3O_4-treated cancer cells. The Mn_3O_4 nanoparticles entered the cell and aggregated in the cytoplasm. To be more precise, the particle aggregates agglomerated and accumulated inside the membrane-bound space that was recognized as destroyed mitochondria[30]. The mitochondria have a swollen morphology with a bright matrix and completely destroyed cristae. Their main function – to produce cellular energy – was blocked, which consequently led to the cell death. It should be pointed out here that similar to SCCVII cells, Mn_3O_4 in L929 and FsaR cells also accumulated in the membrane-bound space (results not shown). Thus, the localization of nanoparticles in cells was not the main reason for selective cytotoxic effect of the Mn_3O_4 nanoparticles.

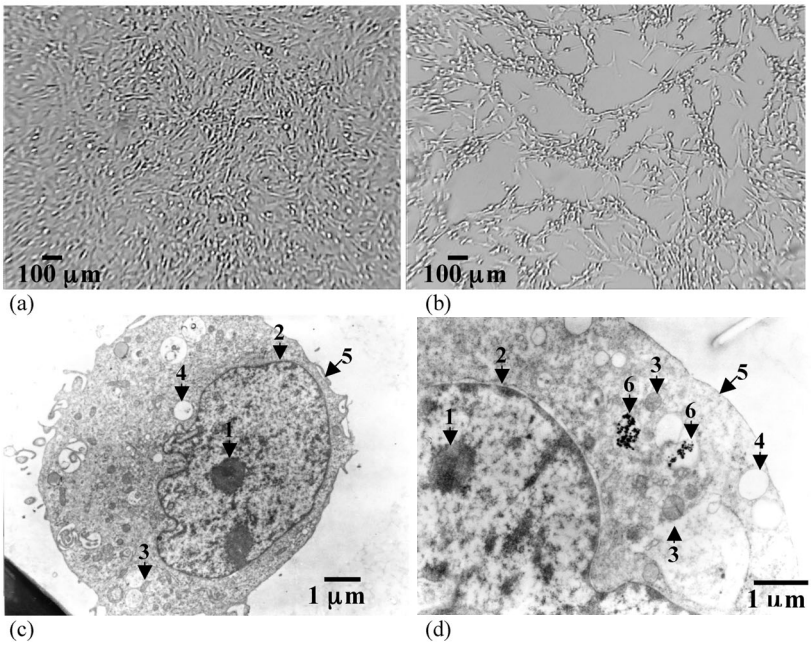

FIG. 4

Images illustrating the cytotoxic effect and sub-cellular accumulation of Mn_3O_4 nanoparticles in cancer cells (SCCVII line). A microphotograph of control cancer cells (a). The effect of addition of the Mn_3O_4 nanoparticles to the SCCVII cell culture; the Mn_3O_4 nanoparticles reduced significantly the number of cancer cells and altered their morphologies (b). A TEM micrograph of control cancer cells; the subcellular structure (1 chromatin, 2 nucleus membrane, 3 mitochondrion, 4 vacuole, 5 cell membrane) of one viable SCCVII cell is visible (c). A TEM micrograph of the Mn_3O_4-treated cancer cell; the Mn_3O_4 nanoparticles entered the cell and aggregated and accumulated inside the membrane-bound space (position 6) recognized as destroyed mitochondria (d)

CONCLUSIONS

The pseudospherical 20-nm Mn_3O_4 nanoparticles were synthesized by optimizing the $MnCl_2/H_2O_2/NH_4OH$ precipitation system. This system is highly sensitive to the concentration of reagents and the order of addition of the precipitating agent.

The Mn_3O_4 nanoparticles were applied to cancer cells. In the concentration range 25–100 μg/ml, the Mn_3O_4 nanoparticles were almost not cytotoxic to L929 fibroblast cells, medium cytotoxic to FsaR fibrosarcoma cells and highly cytotoxic to SCCVII carcinoma cells. Instead of preventing cytotoxicity of Mn_3O_4, NAC increased cytotoxicity of the Mn_3O_4 nanoparticles, suggesting that ROS were not responsible for selective cytotoxic effect of Mn_3O_4 nanoparticles.

It was shown that the Mn_3O_4 nanoparticles entered the cells and aggregated inside the membrane-bound spaces that were recognized as destroyed mitochondria. However, since the Mn_3O_4 nanoparticles localized in all cell lines at similar membrane-bound spaces this should not be the main reason for the selective cytotoxic effect of the Mn_3O_4 nanoparticles.

The authors wish to thank Dr D. Ivanković for performing the Crystal Violet bioassay experiments and Dr N. Ljubešić for his helpful discussion of TEM results.

REFERENCES

1. Gotić M., Popović S., Musić S.: *Mater. Lett.* **1994**, *21*, 289.
2. Gotić M., Musić S., Ivanda M., Šoufek M., Popović S.: *J. Mol. Struct.* **2005**, *744–747*, 535.
3. Gotić M., Ivanda M., Popović S., Musić S.: *Mater. Sci. Eng., B* **2000**, *77*, 193.
4. Gotić M., Popović S., Ljubešić N., Musić S.: *J. Mater. Sci.* **1994**, *29*, 2474.
5. Gotić M., Musić S.: *Eur. J. Inorg. Chem.* **2008**, 966.
6. Gotić M., Ivanda M., Sekulić A., Musić S., Popović S., Turković A., Furić K.: *Mater. Lett.* **1996**, *28*, 225.
7. Gotić M., Popović S., Ivanda M., Musić S.: *Mater. Lett.* **2003**, *57*, 3186.
8. Gotić M., Jurkin T., Musić S.: *Colloid. Polym. Sci.* **2007**, *285*, 793.
9. Ivanda M., Musić S., Popović S., Gotić M.: *J. Mol. Struct.* **1999**, *481*, 645.
10. Šijaković-Vujičić N., Gotić M., Musić S., Ivanda M., Popović S.: *J. Sol-Gel Sci. Technol.* **2004**, *30*, 5.
11. Gotić M., Popović S., Musić S.: *Mater. Lett.* **2007**, *61*, 709.
12. Niederberger M.: *Acc. Chem. Res.* **2007**, *40*, 793.
13. Hu Y., Chen J., Xue X., Li T.: *Mater. Lett.* **2006**, *60*, 383.
14. Yang L.-X., Zhu Y.-J., Tong H., Wang W.-W., Cheng G.-F.: *J. Solid State Chem.* **2006**, *179*, 1225.
15. Chen Z. W., Lai J. K. L., Shek C. H.: *Scr. Mater.* **2006**, *55*, 735.
16. Zhang Y. C., Qiao T., Hu X. Y.: *J. Solid State Chem.* **2004**, *177*, 4093.

17. Gibot P., Laffont L.: *J. Solid State Chem.* **2007**, *180*, 695.
18. Wang Z. H., Geng D. Y., Zhang Y. J., Zhang Z. D.: *J. Cryst. Growth* **2008**, *310*, 4148.
19. Vázquez-Olmos A., Redón R., Rodríguez-Gattorno G., Mata-Zamora M. E., Morales-Leal F., Fernández-Osorio A. L., Saniger J. S.: *J. Colloid Interface Sci.* **2005**, *291*, 175.
20. Özkaya T., Baykal A., Kavas H., Köseoglu Y., Toprak M. S.: *Physica B* **2008**, *403*, 3760.
21. Ivanković S., Gotić M., Jurin M., Musić S.: *J. Sol-Gel Sci. Technol.* **2003**, *27*, 225.
22. Ivanković S., Musić S., Gotić M., Ljubešić N.: *Toxicol. in Vitro* **2006**, *20*, 286.
23. Ishii M., Nakahira M., Yamanaka T.: *Solid State Commun.* **1972**, *11*, 209.
24. Buciuman F., Patcas F., Craciun R., Zahn D. R. T.: *Phys. Chem. Chem. Phys.* **1999**, *1*, 185.
25. Marbán G., Valdés-Solís T., Fuertas A. B.: *Phys. Chem. Chem. Phys.* **2004**, *6*, 453.
26. Musić S., Gotić M., Popović S.: *J. Mater. Sci.* **1993**, *28*, 5744.
27. Unfried K., Albrecht C., Klotz L.-O., Mikecz A. V., Grether-Beck S., Schins R. P. F.: *Nanotoxicology* **2007**, 1.
28. Juzenas P., Chen W., Sun Y.-P., Coelho M. A. N., Generalov R., Christensen I. L.: *Adv. Drug Delivery Rev.* **2008**, *60*, 1600.
29. Hanley C., Layne J., Punnoose A., Reddy K. M., Coombs I., Coombs A., Feris K., Wingett D.: *Nanotechnology* **2008**, *19*, 295103.
30. Pedrycz A., Wieczorski M., Czerny K.: *Environ. Toxicol. Pharmacol.* **2005**, *20*, 157.